Mechanism of formation of hollow fiber membranes for membrane distillation: 1. Inner coagulation power effect on morphological characteristics

L. García-Fernández [1], M.C. García-Payo [1], M. Khayet [1,2,*]

[1] Department of Applied Physics I, Faculty of Physics, University Complutense of Madrid, Av. Complutense s/n, 28040, Madrid, Spain.

[2] Madrid Institute for Advanced Studies of Water (IMDEA Water Institute), Avda. Punto Com nº 2, Alcalá de Henares, 28805, Madrid (Spain).

* Corresponding author: khayetm@fis.ucm.es

Tel. +34-91-3945185

Fax. +34-91-3945191

Abstract

Hollow fiber membrane morphology and inner surface structure were analyzed based on the thermodynamic and kinetics of the phase inversion process. Different nonsolvent mixtures formed by *N,N*-dimethyl acetamide (DMAC) and distilled water were considered. By means of Hansen solubility parameters, lower interaction between the nonsolvent and the mixed solvent (DMAC/trimethyl phosphate, TMP) was observed when greater amount of DMAC was added in the nonsolvent. The spinning solution became thermodynamically more stable and kinetically showed slower coagulation rates, being both related to the resultant membrane formation. In this first study poly(vinylidene fluoride-co-hexafluoropropylene) (PVDF-HFP) hollow fiber membranes were prepared by the dry/wet spinning technique employing the above cited nonsolvent mixtures as an internal coagulant. Their effect on the internal structure of the membrane evolved towards a more open-porous inner surface when increasing the solvent content in the bore liquid. Various characterization techniques were used in order to analyze the adequacy of these membranes for desalination by direct contact membrane distillation (DCMD). It was found that all the properties together with the permeability of the hollow fibers improved when the coagulation power of the nonsolvent was reduced.

Keywords:

Hollow fiber membrane; Membrane Distillation; Membrane morphology; Mixed solvent; Nonsolvent coagulation power; Solvent-nonsolvent interaction

1. Introduction

Membrane distillation (MD) is a non-isothermal process applied mainly to remove non-volatile solutes such as salts from water. Its driving force is the transmembrane water vapor pressure and the most commonly used MD configuration is direct contact membrane distillation (DCMD) [1]. However, one of the main drawbacks of this process is the unavailability of commercial membranes that meet all the MD requirements [2]. Therefore, the design of MD membranes is nowadays an attractive research topic [3-5], despite the great difficulty associated with understanding the mechanism of membrane formation [6]. Some of the main requirements of an adequate MD membrane are the high hydrophobicity, low thermal conductivity and high porosity [1-3].

Cui et al. [7] reported different hydrophobic fluoropolymers and copolymers that can be employed as suitable materials for MD membranes preparation, such as the well known and commonly used polyvinylidene fluoride (PVDF) [8, 9]. Fluoropolymers exhibit excellent properties as materials for a membrane for MD including thermal and chemical resistances [7]. The copolymer poly(vinylidene fluoride-co-hexafluoropropylene) (PVDF-HFP) stands out for its excellent hydrophobic character due to the hexafluoropropylene (HFP) group embedment, as confirmed by several researchers [10, 11]. Not only does the HFP incorporation improve the hydrophobic character of PVDF due to its fluorine content, but also the crystalline character of vinylidene fluoride (VDF) enhances the mechanical properties of the formed material [7]. Therefore, PVDF-HFP is an advisable copolymer to consider for the preparation of MD membranes as confirmed elsewhere [12-14]. The polymeric matrix selection is also important in terms of thermal conductivity. Nevertheless, there is not much difference between the thermal conductivity coefficients of the majority of the available

hydrophobic polymers. That is why the heat transfer by conduction through the membrane must be reduced by enhancing the void volume fraction (i.e. porosity) [2]. High porosity always induces high MD permeability, as it has been confirmed in several studies [1, 2, 13]. Trying to pursue this objective, it is advised by several membranologists to introduce in the dope solution pore former additives such as polyvinylpyrrolidone (PVP), lithium chloride (LiCl), glycerol, polyethylene glycol (PEG), etc [12, 15].

Besides the aforementioned MD membrane main properties, a proper morphology also plays a key role on membrane performance. It would be enhanced if macro-void free structure, skinless and open-porous surfaces conform the membrane morphology [8, 9, 16]. First, in order to obtain the desired structure, it is necessary to analyze the membrane formation process via the thermodynamic and kinetics of the phase inversion, and to understand the consequence of the variation of each fabrication parameter [6, 17-20]. This is even more complicated for hollow fiber membrane preparation, because dry/wet spinning technique involves many fabrication parameters, which directly affect membrane morphology. One of the advantages of using MD hollow fiber membranes is the high packing density that can be easily achieved in tubular membrane modules [1-3].

Several hollow fiber preparation parameters such as spinning dope composition, spinneret dimensions, extrusion pressure, air gap distance, temperatures of the dope and coagulants solutions, coagulants flow rate and composition, take-up speed, etc., can modify the membrane structure [1, 21-23]. Although it has been already studied the effect of solvent/water mixture as nonsolvent on the membrane characteristics [24, 25], no study is found when the coagulant interacts with a mixed solvent instead of a single solvent for preparing PVDF-HFP hollow fiber membranes. The solvents mixture is

formed by two solvents, one is the same main solvent of the nonsolvent aqueous mixtures, and therefore different interaction forces compete between each other simultaneously. The nonosolvent-solvent exchange type during the phase inversion strongly affects hollow fiber membrane morphology and properties as well as membrane performance by MD process. In the first part of this study the solvent-nonsolvent interaction effect on the PVDF-HFP hollow fiber membrane formation mechanism and consequently on its structural cross-section and inner surface morphology have been deeply and exhaustively investigated.

2. Experimental

2.1 Materials

The copolymer poly(vinylidene fluoride-co-hexafluoropropylene) (PVDF-HFP; M_w = 455,000 g/mol), the solvents *N,N*-dimethyl acetamide (DMAC) and trimethyl phosphate (TMP) and the additive poly(ethylene glycol) (PEG; M_w = 6000 g/mol) were used to prepare the spinning solution and were all purchased from Sigma-Aldrich. Isopropyl alcohol (IPA, Sigma-Aldrich) and POREFIL® (Porometer) were employed as wetting liquids for the measurements of the void volume fraction and porometry, respectively. Sodium chloride (NaCl) was employed to prepare the salt aqueous feed solutions for DMCD experiments and it was purchased from Panreac.

2.2 Preparation of hollow fiber membranes

The dry/wet spinning was the fabrication technique employed to prepare all the hollow fiber membranes in this study as it was described elsewhere [26, 27]. First, a unique spinning solution was prepared as follows. 5 wt% of the additive (PEG) was first dissolved in 76 wt% of the solvents mixture at 42ºC and 100 rpm using a magnetic stirrer (IKA, RCT basic), and after getting an homogenous mixture, 19 wt% of PVDF-HFP was added to this mixture. Then, the whole solution was introduced in a thermal

bath (Stuart SBS40) maintained at 42ºC under an orbital shaker until the whole copolymer was totally dissolved. The solvents mixture used to prepare this spinning solution was 40 wt% DMAC and 60 wt% TMP. This mixture was chosen based on the conclusions drawn in our previous study [17].

Table 1 summarizes the spinning parameters, which were maintained the same except the type of the internal coagulant. After spinning, in order to remove the residual solvents, the fabricated hollow fiber membranes were stored in water bath at room temperature for 48 h. Subsequently, the hollow fiber membranes were dried at room temperature before characterization tests. Several mixtures of DMAC and distilled water were used as internal coagulant, employing the following ratios: 0, 20, 40, 50 and 60 wt% of DMAC. The corresponding fabricated hollow fiber membranes are termed here after 1IND0, 1IND20, 1IND40, 1IND50 and 1IND60, respectively.

2.3 Spinning solution characterization prior to membrane fabrication

2.3.1 Physical properties: surface tension, viscosity and Hansen solubility parameters

The surface tension of the spinning solution was measured at room temperature by the pendant drop shape analysis. An optical contact angle meter (CAM 200) and a stainless steel needle with an outer diameter of 1.832 mm were employed to carry out the measurement, keeping constant the drop volume at 12.4 μL for all the samples.

The viscosity of the spinning solution was determined by a Digital Viscometer (Brookfield, Model DV-I+) using the SC4-31 spindle at 4 rpm and a cylindrical sample container. The temperature of the spinning solution was maintained constant at 42 ^{o}C (i.e. the same temperature considered to prepare the hollow fiber membrane) by a thermostat (Techne, Model TU-16D).

Copolymer/solvent/nonsolvent interactions were analyzed via Hansen solubility parameter (*HSP*) distance (R_{HSP}), as it was explained in detail by Hansen [28] and described elsewhere [17]. This parameter informs about the relative affinity between the PVDF-HFP and the solvent, represented by R_{HSP} (P-S); and between nonsolvent (DMAC/water coagulant mixtures) and the mixed solvent, represented by R_{HSP} (NS-S_m). These R_{HSP} values were calculated from the following equations:

$$R_{HSP}(P-S)=\sqrt{4\left(\delta_{d_P}-\delta_{d_S}\right)^2+\left(\delta_{p_P}-\delta_{p_S}\right)^2+\left(\delta_{h_P}-\delta_{h_S}\right)^2} \quad (1)$$

$$R_{HSP}(NS-S_m)=\sqrt{4\left(\delta_{d_{NS}}-\delta_{d_{S_m}}\right)^2+\left(\delta_{p_{NS}}-\delta_{p_{S_m}}\right)^2+\left(\delta_{h_{NS}}-\delta_{h_{S_m}}\right)^2} \quad (2)$$

Before R_{HSP} calculation, it is necessary to know the *HSP* components, which includes the polar component (δ_p), the dispersion force component (δ_d), and the hydrogen bonding component (δ_h) [28]. In Table 2, the *HSP* components of all the pure substances are listed [10, 28, 29], as well as the obtained values of both solvent mixture (S_m) and nonsolvent mixtures (NS), which were calculated from the following equations (3) and (4), respectively [17, 30]:

$$\left[\delta_{dS_m},\delta_{pS_m},\delta_{hS_m}\right]= \left[a\delta_{d1}+b\delta_{d2}+c\delta_{d3},a\delta_{p1}+b\delta_{p2}+c\delta_{p3},a\delta_{h1}+b\delta_{h2}+c\delta_{h3}\right]/(a+b+c) \quad (3)$$

where the subscripts 1, 2 and 3 are for each compound present in the solvent mixture (i.e. DMAC, TMP and PEG) and *a, b* and *c* are the volume fraction of the different compounds in the solvent mixture.

$$\left[\delta_{dNS},\delta_{pNS},\delta_{hNS}\right]=\left[d\delta_{d1}+e\delta_{d2},d\delta_{p1}+e\delta_{p2},d\delta_{h1}+e\delta_{h2}\right]/(d+e) \quad (4)$$

where the subscripts 1 and 2 are for each compound present in the nonsolvent mixture (i.e. DMAC and water) and *d* and *e* are the volume fraction of the different compounds in the nonsolvent mixture.

It is important to highlight that in this study, the additive PEG was also considered as compound in the solvents mixture, together with DMAC and TMP. This additive was treated as solvent (instead of a polymer) for copolymer/solvent/nonsolvent interactions [31, 32] and for thermodynamic experiments analysis [33]. The authors of these mentioned research studies considered that nonsolvent additives and solvents may be considered as unique component. Furthermore, this fact was confirmed via Fourier transform infrared spectroscopy (FTIR); which showed that after phase inversion, other than the solvents, PEG was completely removed from the membrane matrix.

As it is mentioned previously, the proportions of the nonsolvent mixture (DMAC/water) used as internal coagulant were changed for each spinning process. Therefore, R_{HSP} (NS-S_m) was the main parameter considered for comparisons and analysis. The lower is the distance R_{HSP} (NS-S_m), the weaker is the coagulant.

2.3.2 Thermodynamic experiment: cloud point

The thermodynamic behavior during phase inversion membrane formation process can be studied by the ternary phase diagram, where the system copolymer/solvent/nonsolvent was analyzed. The quantity of nonsolvent required to induce copolymer precipitation (i.e. cloud point) was plotted for the same spinning solution (i.e. same copolymer and mixed solvent) but for different nonsolvents (DMAC/water mixtures at different rates). The cloud point was measured by turbidimetric titration method [34]. 50 µl of each nonsolvent mixture was added stepwise to the spinning solution, keeping constant the stirring at 150 rpm and the

temperature at 42 ºC by a magnetic stirrer (IKA, RCT basic) until the dope solution became permanently turbid.

2.3.3 Kinetics experiment: copolymer coagulation

The solvent-nonsolvent exchange rate and the coagulation initiation of the spinning solution were studied by light transmittance test. The experimental device consists of a light-emitting diode (LED) tube lamp employed as light source and a set of Light Dependence Resistances (LDRs) as light detector. The spinning solution was cast and immersed in different nonsolvent (DMAC/water) coagulation baths and the transmitted light evolution was registered by a multimeter (KEITHLEY 199 SYSTEM DMM/SCANNER) connected to a computer. The whole set-up was designed, calibrated and automated by our research group. Both phase inversion initiation and coagulation rate of PVDF-HFP in each coagulation bath were determined by the resultant transmittance curve over the time.

2.4 Characterization of hollow fiber membranes

The morphology of the prepared membranes was studied by the field emission scanning electron microscope (FESEM, JEOL Model JSM-6335F). Previously, the samples were fractured in liquid nitrogen and then sputter-coated (BALZERS SCD 004) with a thin layer (~15 nm) of gold under 20 mA.

The inner and outer diameters of the hollow fibers were measured by an optical microscope (OLYMPUS BX60M) with a precision of ± 1 μm. Both, the void volume fraction (i.e. porosity, ε) and the liquid entry pressure (*LEP*) in the membrane pores were determined following the methods described in previous studies [35, 36]. The porosity of the membranes was measured by the pycnometer gravimetric method as it

was explained in detail elsewhere [37]. In this case, *LEP* measurement was carried out using the procedure and set-up schematized in [17]. The *LEP* results inform about membrane hydrophobicity and its applicability in MD process. The transmembrane operating hydrostatic pressure during MD experiment must be always lower than the *LEP* value, in order to avoid wetting problems.

Another parameter related to the hydrophobic character of the membranes is the water contact angle. Both inner and outer surface contact angles of hollow fiber membranes were measured at room temperature, (30 ± 1) ^{o}C, following the method described by Zhang et al. [38] based on surface tension effects.

The bubble pore size, the mean pore size and the smallest pore size of all the prepared hollow fiber membranes, as well as the cumulative filter flow curves were determined via gas-liquid displacement Porometer and its corresponding computer software (POROLUX™ 100, Porometer). POREFIL® (Porometer) was used as the wetting liquid. The whole followed procedure was described elsewhere [17, 39, 40].

Atomic force microscopy (AFM) was the technique employed to study the mean pore size, the pore size distribution and the roughness of both internal and external surfaces of the prepared hollow fibers. Nanoscope III equipped with 1553D scanner (Digital Instruments Inc., Santa Barbara, Ca) in a tapping mode, provided images, which were treated and analyzed following the same procedure detailed elsewhere [26, 35, 40-42].

The melting (T_m) and the crystallization (T_c) temperatures as well as the enthalpy of melting (ΔH_m) and enthalpy of crystallization (ΔH_c) were obtained from the endothermic and exothermic peaks, respectively; which were determined by the Differential Scanning Calorimetry (DSC) (Mettler-Toledo DSC 1, STAR^{e} System). The

measurements were carried out from 3.25 to 3.73 mg samples that were placed in standard aluminum pans of 100 μl capacity in a nitrogen atmosphere at a flow rate of 60-70 ml/min. The same speed was employed for both heating and cooling at a rate of 15°C/min from 60°C to 200°C. The degree of the crystallinity of the samples was estimated as stated in other studies [17, 43, 44].

The mechanical properties of the hollow fiber membranes were determined at room temperature using an Instron dynamometer (model 3366), according to ASTM D 3379-75 specifications. A load cell of 50 N with a cross-head speed of 80 mm/min and an initial length of the fiber sample of 50 mm were employed. The tensile test of each membrane was repeated for five samples, and the corresponding characteristics were calculated as the average of the five measurements.

2.5 Direct contact membrane distillation experiments

DCMD experiments were carried out using the experimental set-up and the procedure described in detail in [17]. Briefly, six PVDF-HFP hollow fibers were assembled in a shell-and-tube module with an effective length of 20 cm. The feed and permeate circulated tangentially to the membrane in a counter-current way. The feed solution was circulated through the lumen side of the membrane, while the permeate (distilled water) was circulated through the shell side of the module. First, prior to the DCMD experiments, a checking leak test was carried out by circulating distilled water through both the lumen and shell sides of the membrane module at the same temperature confirming that no mass was registered during at least five hours. Subsequently, DCMD experiments were performed with distilled water and a salt aqueous solution (NaCl, 3 wt%) as feed solutions. The feed inlet temperature was 80 °C and that of the permeate was 25 °C. The feed flow rate was kept at 13.8 ± 1.2 kg/h, and

the permeate at 20.7 ± 0.6 kg/h. The permeate flux was calculated based on the mass of water produced over time and the inner fiber surface area. The salt rejection factor was determined measuring the electrical conductivity of both the feed and permeate extracted at the beginning and at the end of each DCMD experiment.

3. Results and discussions

3.1 Spinning solution characterization prior to membrane fabrication

3.1.1 Physical properties: surface tension, viscosity and Hansen solubility parameters

The surface tension obtained for the used dope solution in this study was (30.45 ± 0.20) mN/m. This is an important characteristic parameter to be considered as it affects the hollow fiber diameters and its thickness as consequence. The spinning solution viscosity is related to the kinetics of the phase inversion process, during solvent and nonsolvent interdiffusion. The viscosity of the dope solution prepared for this study was (3688 ± 81) mPa s, which is in the same order of magnitude as other used PVDF-HFP spinning dope solutions in other studies [10, 11, 15].

As it is summarized in Table 2 and represented in Fig. 1(a), the value of R_{HSP} for the pair nonsolvent and solvents mixture (NS-S_m) linearly decreased when DMAC amount in the nonsolvent mixture (DMAC/water) increased. This means that the interaction between nonsolvent and solvent was reduced with the increase of DMAC content, making the solvent-nonsolvent interdiffussion during the phase inversion process slower. It is because the coagulant became weaker when the quantity of solvent increased in DMAC/water mixture as Xu et al. [24] described.

Figure 1(a) also shows the intersection between R_{HSP} (P-S_m) value for the pair PVDF-HFP and DMAC40 and the R_{HSP} (NS-S_m) curve, which represents the DMAC

limit concentration in the nonsolvent mixture for coagulation power effectiveness. The corresponding R_{HSP} (NS-S_m) of the nonsolvent mixtures D70 and D80 were almost equal or even smaller than R_{HSP} (P-S_m), respectively. It means that the mixture D70 could hardly been able to induce the phase inversion of the copolymer, being impossible its coagulation if the nonsolvent D80 was used. The conclusions obtained from the Hansen solubility analysis could predict the possibility/impossibility of a membrane phase inversion formation according the polymer/solvent/nonsolvent interactions.

ΔR_{HSP} (NS-S) dependence on the DMAC concentration in the nonsolvent mixture is shown in Fig. 1(b). ΔR_{HSP} (NS-S) represents the difference between the R_{HSP} value for the pair nonsolvent mixture and mixed solvent (NS-S_m) and the R_{HSP} value for the pair nonsolvent mixture and each individual solvent (NS-S_i). This parameter was calculated from the following equation:

$$\Delta R_{HSP}(NS-S)_i = R_{HSP}(NS-S_m) - R_{HSP}(NS-S_i) \quad (5)$$

where the subscript *i* is for each solvent, DMAC or TMP.

Interesting conclusions can be drawn from Fig. 1(b). Nonsolvent-solvent affinity improved when the solvents mixture was used instead of each solvent individually. This was expressed as the negative values of the calculated parameter ΔR_{HSP} (NS-S) (i.e. R_{HSP} (NS-S_m) < R_{HSP} (NS-S_i)). ΔR_{HSP} (NS-S) < 0 were obtained for all the DMAC concentrations in the nonsolvent mixture ranging from 28 to 75 wt% approximately, for both DMAC and TMP solvents. However, for DMAC concentrations below 28 wt% in the nonsolvent, using the TMP as individual solvent would enhance the nonsolvent-solvent affinity; and for DMAC concentrations higher than 75 wt% in the nonsolvent, DMAC would be more advisable to use as a single solvent (i.e. in both cases ΔR_{HSP}

(NS-S) > 0). On the other hand, in the concentration range 28 – 75 wt% DMAC, $|\Delta R_{HSP}(NS-S)_{TMP}| < |\Delta R_{HSP}(NS-S)_{DMAC}|$ for DMAC content in the nonsolvent lower than 50 wt% and $|\Delta R_{HSP}(NS-S)_{TMP}| > |\Delta R_{HSP}(NS-S)_{DMAC}|$ for DMAC content greater than 60 wt%, as shown Fig. 1(b). Therefore, for low concentrations of DMAC in the nonsolvent below 50 wt%, R_{HSP} (NS-S_m) is closer to R_{HSP} (NS-S_{TMP}) than to R_{HSP} (NS-S_{DMAC}). This means that for these DMAC concentrations, TMP is the predominant solvent of the mixture that intervenes more in the NS-S_m interaction. An opposite but more pronounced behavior was observed for higher concentrations of DMAC (above 60 wt%), concluding that the solvent DMAC is the predominant solvent of the mixture influencing the NS-S_m interaction. Furthermore, the calculated values of ΔR_{HSP} (NS-S) for each solvent were similar for DMAC concentrations in the nonsolvent mixture between 50 and 60 wt%. This indicates that in this range both solvents represented a similar power for nonsolvent-solvent interaction and their influences on the nonsolvent would be compensated. Consequently, slower NS-S_m exchange rate occurred, resulting in the most promising conditions for an appropriate membrane design as porous and sponge-like structure could be obtained.

3.1.2 Thermodynamic and kinetics experiments

The thermodynamic of the spinning solution during the phase inversion process was represented in the ternary phase diagram (see Fig. 2). In this study, a unique dope solution was analyzed; however, the nonsolvent solution was changed increasing the amount of DMAC in DMAC/water mixture. It was observed that when the content of DMAC in water was increased, the cloud point shifted away from PVDF-HFP – solvent axis towards PVDF-HFP – nonsolvent axis; and this effect was much more pronounced for the highest DMAC concentrations (70 and even more for 80%). It means that larger

quantity of nonsolvent was needed for PVDF-HFP precipitation. The results of these thermodynamic experiments agrees with the R_{HSP} (NS-S_m) trend in Fig. 1(a), showing that increasing the amount of DMAC in water, the nonsolvent become weaker and consequently the coagulation process starts later. Xu et al. [45] observed the same direction displacement of the binodal line when the content of DMAC in the nonsolvent increased for the system poly(ether imide) (PEI)/DMAC/DMAC+water. This result showed a delayed demixing phase separation process when greater quantity of DMAC was used in the internal coagulant.

The kinetics experiments were carried out via light transmission test, employing the same dope solution and changing the nonsolvent mixture. The obtained demixing curves are represented in Fig. 3. The curves show the appearance of three different stages during the coagulation process as it was also reported by Li et al. [31, 46]. In the first stage there is a slight decrease of the transmittance, showing a delay in the nonsolvent penetration into the copolymeric cast film. In the second stage, the curve´s slope changes abruptly indicating the beginning and the rate of the demixing process. Finally, in the third stage the transmittance reduces approaching an asymptotic transmittance value indicating the end of the demixing process. By increasing the quantity of DMAC in the nonsolvent mixture, the registered time for the first stage became longer and the slope of the curve in the second stage decreased. These mean that due to the weaker coagulant, the initiation of the phase inversion was delayed and the coagulation rate became slower, being the three stages indistinguishable when the highest percentage of DMAC (60 wt%) was used in the nonsolvent mixture. This result is related to the solubility parameter difference and the thermodynamic results (i.e. the lower R_{HSP} (NS-S_m) is the longer the time to occur the cloud point is and the slower the coagulation is too). Both parameters indicated that increasing the amount of DMAC in

the nonsolvent mixture the coagulation started later and the process was slower. Similar light transmittance´s curves tendency (i.e. lower precipitation rate) was obtained by Zhang et al. [47] when polyvinyl butyral (PVB) dope solutions came into contact with DMAC/water coagulation baths. Machado et al. [6] who studied the membrane formation mechanism of flat-sheet polysulfone (PSf) membranes explained that increasing the solvent concentration in the coagulation bath diminished the driving force responsible to leach out the solvent from the polymeric solution, inducing longer liquid-liquid demixing process as consequence.

It is to be noted that when employing higher quantities of DMAC (i.e. 70 and 80 wt%) in the nonsolvent DMAC/water mixture for light transmittance experiments, it was impossible to observe membrane phase inversion. This may be attributed to the extremely weakness properties of these coagulants when higher quantity of DMAC (over 60 wt%) was used in DMAC/water nonsolvent mixture. As it was predicted by R_{HSP} (NS-S_m) results (see the limit concentration of coagulation at Fig. 1(a)) and the cloud point experiments, with both mixtures the copolymer in the dope solution tends to be dissolved instead of coagulating. From the qualitative model developed for flat-sheet polymeric membranes by Machado et al. [6], the precipitation rate greatly decreased tending to dissolve the polymer for very high solvent concentration in the coagulation bath. Therefore, in light of all the previous characterization results, it was concluded that preparing PVDF-HFP hollow fiber membranes under the same experimental conditions and employing these mixed coagulants (i.e. D70 and D80) would be impossible. This was experimentally verified using these mixtures as bore liquids to prepare hollow fiber membranes. It was observed that the nonsolvent mixture D70 used as the internal coagulant of the spinning process was not able to form the hollow fiber membrane shape although phase inversion was occurred. Nevertheless, the copolymer

coagulation was impossible using D80 as the bore liquid and the phase inversion did not take place.

3.2 Hollow fiber membrane characterization

3.2.1 Morphology of the hollow fiber membranes prepared with different internal coagulants

The cross-section and the internal surface of the hollow fiber membranes were analyzed by SEM and the corresponding images can be seen in Fig. 4. These illustrate the effect of the internal coagulant by analyzing the evolution of the internal structure of the membranes prepared with different internal coagulants (i.e. different amount of DMAC in DMAC/water mixtures). In general, all the membranes present common asymmetric cross-section morphology, a sponge-like structure in the middle and a finger-like structure in the external and/or internal layers. When water was used as a bore fluid, long fingers ended by voids grew from the inner layer to the middle of the fiber cross-section, while short fingers appeared in the outer layer. Increasing DMAC concentration in DMAC/water mixture modified both the cross-section and the inner surface structure of the membranes. The fingers of the outer layer became longer while the fingers of the inner layer became shorter, changing therefore the thickness of the middle sponge-like structure. This effect on membrane morphology was also observed by Xu et al. [24] when low concentrations of DMAC (i.e. 0, 10, 20 and 30 wt%) in water were used as internal coagulant for the fabrication of the PVDF hollow fibers. Besides the structure of the PVDF-HFP membranes prepared for the present study, from SEM images a thinner hollow fiber cross-section was detected for the membranes prepared with higher DMAC content in the DMAC/water mixture. This will be explained in the following 3.2.2 section.

Porous inner surfaces were observed for all the fabricated membranes. The largest internal surface pore sizes were observed for the membranes 1IND50 and 1IND60, when the greatest amounts of DMAC were used in the bore liquid, as it will be confirmed by means of AFM analysis. The thermodynamic experiment results could explain the skinless inner surfaces of the prepared hollow fibers [45]. When DMAC concentration in the internal coagulant was increased, the cloud point was greater. This means that more quantity of nonsolvent can be incorporated to the dope solution, resulting in a greater amount of solvent in the nascent inner layer of the hollow fiber during the spinning process. The solvent inflow from the bore liquid may decrease the local polymer concentration on the inner interface, preventing the formation of the dense skin-layer and obtaining a more open-porous inner surface structure [25, 48]. It is worth quoting that a skinless and open microporous inner surface of the PSf hollow fiber membranes was detected by Rahbari-sisakht et al. [25] when 1-Methyl-2-pyrrolidone (NMP)/water mixture was used as the bore liquid. By increasing the NMP content from 50 to 90 wt%, the inner surface became more porous with larger pores. Zhang et al. [47] also observed a porous inner surface structures of PVB hollow fibers, when high solvent amounts were added in the internal coagulants. Furthermore, as it can be seen in Fig. 4, all the inner surfaces exhibited a stretched morphology due to the gravity force that elongated the fiber along the gap distance. This stretching effect was more pronounced when increasing the DMAC concentration in the bore liquid. The nascent hollow fibers prepared with a high amount of DMAC in the internal coagulant were not coagulated very fast along the air gap leading to a great stretching effect of the hollow fiber.

As it can be seen in Fig. 4, all the outer surfaces of the PVDF-HFP hollow fibers presented similar dense skin-layer as a consequence of the dry phase inversion step of

the spinning process (i.e. solvent evaporation along the air gap distance) [48-50]. The aforementioned consequences of the higher cloud point also explained the larger fingers observed at the outer layer of the fiber when DMAC content in the internal coagulant mixture was increased. By increasing the DMAC concentration in the bore liquid the nascent membrane was less coagulated along the gap distance. Then, when the hollow fiber reached the water bath, the coagulation process became faster and the inflow of water from the outer layer of the membrane induced the formation and growth of longer fingers from the external layer.

It is worth noting that the fingers of the internal layer disappeared when the highest quantity of DMAC (i.e. 60 wt%) was used, resulting in the most spongy inner layer (see 1IND60 cross-section in Fig. 4) and the most open-porous inner surface structure (see 1IND60 inner surface in Fig. 4). Therefore, it may be expected a higher MD performance for the membrane 1IND60 [8, 18, 23, 51]. It is well known that a sponge-like structure corresponds to a lower coagulation rate whereas a finger-like structure represents a faster solvent-nonsolvent exchange during the coagulation process [17, 24, 35, 46]. The observed changes of the inner structure of the hollow fibers are related with the characteristics of the dope solution discussed previously. The solubility parameter distance between the nonsolvent and the solvents mixture (R_{HSP} (NS-S_m)) was decreased while the cloud point was increased and the coagulation rate was slower when the quantity of DMAC in DMAC/water mixture was increased. In other words the internal coagulant became weak with less interaction with the solvent, delaying the precipitation initiation and slowing down the coagulation during the phase inversion process [24, 52]. Wang et al. [9] also justified the formation of the sponge-like structure near the inner skin of the PVDF hollow fiber membranes by the delayed phase inversion, caused by the use of the bore liquid mixture, NMP/water (80:20).

3.2.2 Structural properties of hollow fiber membranes prepared with different internal coagulants

Table 3 summarizes the inner and outer diameters as well as the thickness of all the prepared hollow fiber membranes in this study. There is no clear effect on either the internal or external diameters when the amount of DMAC is increased. However, as it was observed from SEM cross-section images (Fig. 4), the thickness of the membranes certainly decreased. For 1IND50 and 1IND60 membranes, the thickness was half that of the 1IND0. Shi et al. [11] observed the same effect for the PVDF-HFP hollow fiber membranes. This result may be attributed to the decrease of the bore liquid coagulation power, when a greater solvent quantity was considered. These weaker internal coagulant mixtures were able to precipitate the spinning solution very slowly, as it was predicted by the dope solution characterization experiments, and through the air gap distance due to the stretching of the fiber that was not completely coagulated, the thickness was reduced as consequence.

The void volume fraction or porosity and *LEP* measurements of the hollow fiber membranes are shown in Table 3. The porosity of the membranes increased while the *LEP* decreased when larger amount of DMAC in water was used as internal coagulant mixture. The hollow fiber membrane 1IND0 was out of these trends. This is attributed to the large and numerous fingers of the inner layer that ended by voids in the middle of the fiber cross-section. These induced a higher porosity and a lower *LEP* as it was indicated in [16]. The fiber prepared with the highest amount of DMAC (i.e. membrane 1IND60) resulted to be the most porous membrane. This was justified due to the above mentioned open-porous structure of the inner layer (see SEM cross-section morphology, Fig. 4). The void volume fraction of this membrane was greater than the highest value obtained by García-Payo et al. [13] for the PVDF-HFP hollow fiber membrane prepared

with the lowest copolymer concentration (i.e.17 wt%). A similar effect was detected by Rahbari-sisakht et al. [25] when a mixed bore liquid (NMP/water) was employed for PSf membrane fabrication. The overall porosity increased from 62.0 to 71.7 % when a 50 wt% of NMP was employed instead of water.

As it can be observed in Fig. 4, when DMAC content in the bore liquid was increased the inner surface pore size became larger and bigger fingers were detected in the external layer of the fiber cross-section. These explain the decrease of the *LEP* with the DMAC content in the bore liquid. It is worth noting that the obtained *LEP* values were higher than 1 bar, confirming that all the prepared membranes can be applied in MD technology. These *LEP* values are in the same range as that reported for other PVDF-HFP fibers used for DCMD [13] but higher than those determined for all the PVDF-HFP hollow fiber membranes considered for the experimental design developed by Khayet et al. [21].

Both inner and outer contact angle measurements are also collected in Table 3. No clear trend was observed between these values and the internal coagulant mixtures used for hollow fiber membrane preparation. However, it can be observed that the inner contact angles were much larger than outer contact angles. The same result was observed by Zhang et al. [38] for fluorinated hydrocarbon hollow fiber when using the same contact angle measurement procedure. The very high inner contact angles obtained in this study show that the inner layers of theses fibers have similar hydrophobicity to the polytetrafluoroethylene (PTFE) flat-sheet membrane reported by Zhang et al. [53]. The obtained results for the outer contact angles can be compared to the dynamic contact angles of other fibers measured by a tensiometer. All the membranes prepared in this study have similar outer contact angles to those of other PVDF-HFP hollow fibers [10], but higher than the water contact angle of the PVDF

commercial membrane analyzed by Shi et al. [11]. This result confirms the hydrophobic character enhancement of the PVDF-HFP membrane due to the HFP group addition to the PVDF chain.

The pore sizes of the hollow fiber membranes obtained by means of Porometry test are shown in Table 4. These values were higher than the average pore size of the PVDF-HFP hollow fiber membranes prepared by Wongchitphimon et al. [10]. When the amount of DMAC in the internal coagulant mixture was increased, the bubble pore size was gradually increased, while both the mean and smallest pore sizes became significantly bigger for the fibers prepared with the highest amount of DMAC in water as inner coagulant. This means that not only greater pore sizes were obtained, but also pore size distributions were wider, as shown in Fig. 5 when higher amount of DMAC was used in the internal coagulant. A similar effect was observed by Zhang et al. [54] for the yttria-stabilized zirconia (YSZ) fibers pore size distributions when NMP/water mixtures with higher amount of solvent were used as internal coagulants. The narrowest pore size distribution corresponded to the membrane prepared with pure water as nonsolvent. This was also observed in this study for PVDF-HFP hollow fibers. The mean pore size of the aforementioned YSZ membranes and the PSf hollow fibers prepared by Rahbari-sisakht et al. [25] also increased with increasing the NMP content in the bore liquid.

Figure 6 shows the 3D AFM images of the inner surface of the hollow fiber membranes prepared with different internal coagulant mixtures and Table 5 summarizes the roughness of both the inner and outer surfaces of hollow fibers. No tendency was detected for the mean roughness of the outer surface. If the standard deviations are taken into account, all the values can be considered similar, which is in accordance with the presence of the skin-layer in the external surfaces of all the prepared membranes

(see Fig. 4) as discussed earlier. Similar roughness values were obtained for the outer surface of other PVDF-HFP hollow fiber membranes, which were also prepared with a large air gap distance [13, 55]. Nevertheless, the inner surface of the membranes became significantly rougher when increasing the DMAC quantity in the bore liquid (DMAC/water mixture) up to 60 wt% (see 1IND60 in Fig. 6). This effect on the fiber surface roughness may be related to the open-pore, sponge inner layer structure, and formation of bigger nodules.

The mean pore size and the corresponding standard deviation of the inner surfaces were analyzed (Table 6). All these values were higher than those determined for the inner surface of other PVDF-HFP hollow fiber membranes prepared with different copolymer concentrations and distilled water as a bore liquid [13]. Greater pores were found on the internal surface of the membranes prepared with higher amounts of DMAC (50 and 60 wt%) in the bore liquid. This result was previously observed from the corresponding SEM surface images (see Fig. 4). Figure 7 shows the cumulative pore size distributions and the probability density functions of the corresponding surfaces. It can be seen that the curves of the membranes 1IND50 and 1IND60 shift towards bigger surface pore sizes coinciding with the mean values presented in Table 6.

Figure 8 and Table 7 summarize the thermal properties of the hollow fiber membranes measured by DSC. Both melting and crystallization temperatures and the corresponding enthalpies, of the hollow fiber membranes fabricated with different internal coagulants, were found to be similar to each other and to the copolymer, PVDF-HFP. This result proved that the bore liquid did not affect either the thermal properties or the crystallinity of the membranes. The melting temperatures as well as the corresponding enthalpies fell within the data range of PVDF-HFP, included in Handbook of Polymers [56], 125 – 164 ^{o}C and 36 – 65 J/g, respectively. It is to point

out that the maximum DCMD operating temperature considered in this study was 80 ºC, much lower than both T_m and T_c obtained for all PVDF-HFP hollow fiber membranes; ensuring that the fibers did not suffer any thermal deterioration during DCMD process.

MD technology does not require the use of membranes with very high mechanical properties compared to other pressure-driven membrane processes (Microfiltration, Ultrafiltration, Nanofiltration and Reverse Osmosis). The transmembrane hydrostatic pressure applied in MD is smaller. However, it is important to know the mechanical characteristics of the membranes in order to guarantee a good packing of the membranes in modules [1, 3]. The obtained stress-strain experiments are plotted in Fig. 9 and from these curves the main mechanical parameters were calculated (see Table 8). The Young´s modulus (E) represents the stiffness of the hollow fiber membranes. The E parameter values summarized in Table 8 were higher than those reported by Shi et al. [11] and Wongchitphimon et al. [10] for other PVDF-HFP hollow fiber membranes. By increasing the DMAC concentration in the internal coagulant mixture, E was reduced and the membranes became more elastic. This effect may be related to the increase of fiber´s porosity (see Table 3), facilitating the polymeric chains movement during the stress-strain experiments. The same behavior was detected by Shi et al. [11] when PVP was added into the PVDF-HFP spinning solution. Nevertheless, the E parameter obtained for the membrane prepared with the highest amount of DMAC in the bore liquid (1IND60) did not follow this tendency, it was higher than the Young´s modulus of the hollow fiber 1IND50. In fact, these two membranes had similar porosities. Hence, it may be the change in membrane morphology the responsible of the elasticity difference. As it can be observed in Fig. 4, the fiber 1IND60 is totally free of fingers at the inner layer and exhibits larger sponge-like structure along its cross-section than the membrane 1IND50, making the fiber a little more rigid [15]. The yield and the tensile

stress at break were also analyzed, and both were decreased when the amount of DMAC was higher in the internal coagulant. These results indicate the reduction of the stress held before leaving the elastic region and fracture. The observed decrease of tensile stress at break may be due to the thickness decrease (see Table 3) when a weaker coagulant was used as a bore liquid [5, 39]. However, for both membranes, 1IND50 and 1IND60, with a similar thickness, the yield and the tensile stress at break of 1IND60 were slightly higher than those of the membrane 1IND50. This might be attributed to the inner layer sponge-like structure of 1IND60 and to its stronger and better interconnected inner surface. It is worth noting that all the prepared PVDF-HFP membranes had a tensile stress at break similar or even higher than the reported value of other hollow fibers [10, 11, 15, 57]. The strain at break of the hollow fiber membranes decreased following the same tendency than the tensile stress at break. These values were all lower than the strain at break data of PVDF-HFP fibers reported in other studies [10, 11, 15] but higher than the strain at break of the PVDF commercial hollow fiber (i.e. 128 ± 16 %), tested by Shi et al [11]. It was stated that the observed ductile behavior improvement of all the PVDF-HFP fibers compared with PVDF ones was due to the amorphous group HFP embedment in the PVDF polymeric structure [11].

3.3 DCMD experiments of hollow fiber membranes prepared with different internal coagulants

In order to compare the DCMD performance of the prepared membranes, the permeate fluxes (J) and the salt rejection factors (α) are presented in Fig. 10. As it was expected, the obtained permeate fluxes when distilled water was used as feed were higher than those corresponding to the feed salt aqueous solution (NaCl, 3 wt%) and all hollow fiber membranes exhibited good salt rejection factors. It is worth noting the good fabrication reproducibility of the hollow fiber membranes prepared in this study. It

was confirmed by SEM that the membranes prepared in different batches had the same morphology, and as it is shown in Fig. 10, the obtained DCMD permeate fluxes are within the error range. The permeate fluxes presented in Fig. 10 were greater than the maximum DCMD fluxes reported for other PVDF-HFP hollow fiber membranes (i.e. 1.3 kg/m^{2}h for distilled water as feed at 45 ^{o}C and a permeate temperature of 20 ^{o}C; 6.5 kg/m^{2}h for distilled water as feed at 80 ^{o}C and a permeate temperature of 25 ^{o}C; 5.4 kg/m^{2}h for 3 wt% NaCl feed solution at 80 ^{o}C and a permeate temperature of 25 ^{o}C) [13, 55]. According to the membrane characterization results and the obtained DCMD fluxes, it can be concluded that the use of a mixed internal coagulant improves the hollow fiber morphology, properties and DCMD performance, as consequence. The permeate flux enhancement was not very noticeable when water was changed for 20 wt% DMAC/water or 40 wt% DMAC/water mixtures as internal coagulants. Practically similar DCMD permeate fluxes were obtained for the membranes, 1IND20 and 1IND40, which was totally in accordance with their similar main characteristics such as cross-section structure, inner surface morphology, and mean pore size. However, a sharp increase of the permeate flux was observed when the highest amounts of DMAC (50 and 60 wt%) were used in the bore liquid mixture (DMAC/water). The permeate fluxes of the membranes 1IND50 and 1IND60 were almost doubled due to various reasons. Compared to the membrane 1IND0, the thickness of 1IND50 and 1IND60 membranes decreased around 50%, the porosity became nearly a 20% higher, and the pore sizes were approximately a 70% greater. Furthermore, these hollow fibers had more open porous inner surfaces with larger pores, and especially the membrane 1IND60 exhibited a thicker sponge-like structure more open at the immediately inner layer with a higher mean roughness of the inner surface. All the aforementioned characteristics totally justified the observed greater permeate fluxes of these two hollow

fiber membranes, 1IND50 and 1IND60 [5, 13, 16, 17]. These DCMD permeate fluxes were similar to those exhibited by the optimal PVDF-HFP hollow fiber membrane developed by a statistical experimental design (i.e. 13.5 kg/m^{2}h for 3 wt% NaCl feed aqueous solution at 75 ^{o}C and a permeate temperature of 20 ^{o}C) [21]. It is necessary to highlight that these hollow fiber membranes had excellent salt rejection factors, 99.76% (1IND50) and 99.94% (1IND60) although their maximum pore size were greater than that of the other fibers.

4. Conclusions

The selection of the nonsolvent type for PVDF-HFP hollow fiber membrane preparation strongly affected the membrane morphology, its structural characteristics, and DCMD performance. It was demonstrated that the morphology of these fibers was determined by the quantity of DMAC in water used as an internal coagulant for their preparation. As it was predicted by the spinning solution characterization techniques, the resultant membrane morphology directly depends on the nonsolvent-solvent interactions and thermodynamic and kinetics of membrane phase inversion. The usefulness and validity of the Hansen solubility parameter distance analysis prior membrane preparation was demonstrated. This procedure can be applied to any phase inversion membrane prepared with different spinning solutions and coagulants minimizing therefore the number of the experiments.

It was observed that the higher was the quantity of DMAC in the nonsolvent mixture, the weaker was the internal coagulant, and the earlier and slower was the phase inversion of the membrane. Therefore, more porous inner surfaces with larger pore sizes were formed and the finger-like structure of the inner layer was reduced or even

disappeared forming an open-spongy structure when the greatest content of DMAC was used in the bore liquid.

Other structural characteristics of the hollow fibers were enhanced when the solvent concentration was increased in the internal coagulant such as the lower thickness, higher porosity, larger pore size, narrower inner surface pore size distribution and higher inner surface roughness. The larger bubble pore sizes resulted in lower *LEP* values.

In general, all the prepared membranes exhibited adequate thermal and mechanical properties for MD application. The most significant improvements were obtained for the hollow fibers prepared with the highest concentrations of DMAC in the bore liquid mixtures. The corresponding membranes (1IND50 and 1IND60) were the thinnest and the most porous with the largest pore sizes, leading to the greatest DCMD permeate fluxes and maintaining high salt rejection factors during desalination by DCMD. These results might be even improved if the skin-layer could be removed from the outer surface of these PVDF-HFP hollow fiber membranes. This is the main objective of the next research study [58].

Acknowledgements

The authors are thankful to the financial support of the Ministry of Economy and Competitiveness (MEC) (CTM2015-65348-C2-2-R). L. García-Fernández gratefully acknowledges the Ministry of Education, Culture and Sports, Spain (MECD) for the FPU grant (FPU12/02817).

References

[1] M. Khayet, T. Matsuura, Membrane Distillation. Principles and Applications, Elsevier, The Netherlands (2011).

[2] M. Khayet, Membranes and theoretical modeling of membrane distillation: a review, Adv. Colloid Interface Sci. 164 (2011) 56-88.

[3] L. García-Fernández, M. Khayet, M.C. García-Payo, Membranes used in membrane distillation: preparation and characterization, Elsevier (Woodhead Publishing), Cambridge (2015) 317-359.

[4] M. Qtaishat, M. Khayet, T. Matsuura, Guidelines for preparation of higher flux hydrophobic/hydrophilic composite membranes for membrane distillation, J. Membr. Sci. 329 (2009) 193-200.

[5] M. Essalhi, M. Khayet, Self-sustained webs of polyvinylidene fluoride electrospun nanofibers at different electrospinning times: 1. Desalination by direct contact membrane distillation, J. Membr. Sci. 433 (2013) 167-179.

[6] P.S.T. Machado, A.C. Habert, C.P. Borges, Membrane formation mechanism based on precipitation kinetics and membrane morphology: flat and hollow fiber polysulfone membranes, J. Membr. Sci. 155 (1999) 171-183.

[7] Z. Cui, E. Drioli, Y.M. Lee, Recent progress in fluoropolymers for membranes, Prog. Polym. Sci. 39 (2014) 164-198.

[8] S. Bonyadi, T.S. Chung, Highly porous and macrovoid-free PVDF hollow fiber membranes for membrane distillation by a solvent-dope solution co-extrusion approach, J. Membr. Sci. 331 (2009) 66-74.

[9] K. Yu Wang, T.S. Chung, M. Gryta, Hydrophobic PVDF hollow fiber membranes with narrow pore size distribution and ultra-thin skin for the fresh water production through membrane distillation, Chem. Eng. Sci. 63 (2008) 2587-2594.

[10] S. Wongchitphimon, R. Wang, R. Jiraratananon, L. Shi, C.H. Loh, Effect of polyethylene glycol (PEG) as an additive on the fabrication of polyvinylidene fluoride-

co-hexafluropropylene (PVDF-HFP) asymmetric microporous hollow fiber membranes, J. Membr. Sci. 369 (2011) 329-338.

[11] L. Shi, R. Wang, Y. Cao, C. Feng, D.T. Liang, J.H. Tay, Fabrication of poly(vinylidene fluoride-co-hexafluropropylene) (PVDF-HFP) asymmetric microporous hollow fiber membranes, J. Membr. Sci. 305 (2007) 215-225.

[12] C. Feng, R. Wang, B. Shi, G. Li, Y. Wu, Factors affecting pore structure and performance of poly(vinylidene fluoride-co-hexafluoro propylene) asymmetric porous membrane, J. Membr. Sci. 277 (2006) 55-64.

[13] M.C. García-Payo, M. Essalhi, M. Khayet, Effects of PVDF-HFP concentration on membrane distillation performance and structural morphology of hollow fiber membranes, J. Membr. Sci. 347 (2010) 209-219.

[14] B.S. Lalia, E. Guillen, H.A. Arafat, R. Hashaikeh, Nanocrystalline cellulose reinforced PVDF-HFP membranes for membrane distillation application, Desalination 332 (2014) 134-141.

[15] L. Shi, R. Wang, Y. Cao, D.T. Liang, J.H. Tay, Effect of additives on the fabrication of poly(vinylidene fluoride-co-hexafluropropylene) (PVDF-HFP) asymmetric microporous hollow fiber membranes, J. Membr. Sci. 315 (2008) 195-204.

[16] M.M. Teoh, T.S. Chung, Membrane distillation with hydrophobic macrovoid-free PVDF–PTFE hollow fiber membranes, Sep. Purif. Technol. 66 (2009) 229-236.

[17] L. García-Fernández, M.C. García-Payo, M. Khayet, Effects of mixed solvents on the structural morphology and membrane distillation performance of PVDF-HFP hollow fiber membranes, J. Membr. Sci. 468 (2014) 324-338.

[18] N. Peng, N. Widjojo, P. Sukitpaneenit, M.M. Teoh, G. Glenn Lipscomb, T.S. Chung, J.Y. Lai, Evolution of polymeric hollow fibers as sustainable technologies: Past, present, and future, Prog. Polym. Sci. 37 (2012) 1401– 1424.

[19] P. van de Witte, P.J. Dijkstra, J.W.A. van den Berg, J. Feijen, Phase separation processes in polymer solutions in relation to membrane formation, J. Membr. Sci. 117 (1996) 1-31.

[20] A.C. Sun, W. Kosar, Y. Zhang, X. Feng, A study of thermodynamics and kinetics pertinent to formation of PVDF membranes by phase inversion, Desalination 309 (2013) 156-164.

[21] M. Khayet, C. Cojocaru, M. Essalhi, M.C. García-Payo, P. Arribas, L. García-Fernández, Hollow fiber spinning experimental design and analysis of defects for fabrication of optimized membranes for membrane distillation, Desalination 287 (2012) 146-158.

[22] Y. Tang, N. Li, A. Liu, S. Ding, C. Yi, H. Liu, Effect of spinning conditions on the structure and performance of hydrophobic PVDF hollow fiber membranes for membrane distillation, Desalination 287 (2012) 326-339.

[23] C.Y. Feng, K.C. Khulbe, T. Matsuura, A.F. Ismail, Recent progresses in polymeric hollow fiber membrane preparation, characterization and applications, Sep. Purif. Technol. 111 (2013) 43–71.

[24] A. Xu, A. Yang, S. Young, D. deMontigny, P. Tontiwachwuthikul, Effect of internal coagulant on effectiveness of polyvinylidene fluoride membrane for carbon dioxide separation and absorption, J. Membr. Sci. 311 (2008) 153-158.

[25] M. Rahbari-sisakht, A.F. Ismail, T. Matsuura, Effect of bore fluid composition on structure and performance of asymmetric polysulfone hollow fiber membrane contactor for CO2 absorption, Sep. Purif. Technol. 88 (2012) 99-106.

[26] M. Khayet, The effects of air gap length on the internal and external morphology of hollow fiber membranes, Chem. Eng. Sci. 58 (2003) 3091-3104.

[27] M. Khayet, M.C. García-Payo, F.A. Qusay, M.A. Zubaidy, Structural and performance studies of poly(vinyl chloride) hollow fiber membranes prepared at different air gap lengths, J. Membr. Sci. 330 (2009) 30-39.

[28] C.M. Hansen, Hansen Solubility Parameters: A User´s Handbook, 2nd ed., CRC Press, Taylor & Francis Group, Boca Ratón, FL (2007).

[29] J.E. Mark (Ed.), Polymer Data Hanbook, Oxford University Press (1999).

[30] S. Abbott, C.M. Hansen, H. Yamamoto, Hansen Solubility Parameters in Practice-Complete with Software, Data, and Examples, 3rd ed., Ebook, available from www.hansen-solubility.com (2010).

[31] Q. Li, Z.L. Xu, L.Y. Yu, Effects of mixed solvents and PVDF types on performances of PVDF microporous membranes, J. Appl. Polym. Sci. 115 (2010) 2277-2287.

[32] L. Setiawan, R. Wang, L. Shi, K. Li, A.G. Fane, Novel dual-layer hollow fiber membranes applied for forward osmosis process, J. Membr. Sci. 421-422 (2012) 238-246.

[33] A.F. Ismail, L.P. Yean, Review on the development of defect-free and ultrathin-skinned asymmetric membranes for gas separation through manipulation of phase inversion and rheological factors, J. Appl. Polym. Sci. 88 (2003) 442–451.

[34] M.L. Yeow, Y.T. Liu, K. Li, Isothermal phase diagrams and phase-inversion behaviour of poly(vinylidene fluoride)/solvents/additives/water systems, J. Appl. Polym. Sci. 90 (2003) 2150-2155.

[35] M. Khayet, C.Y. Feng, K.C. Khulbe, T. Matsuura, Preparation and characterization of polyvinylidene fluoride hollow fiber membranes for ultrafiltration, Polymer 43 (2002) 3879-3890.

[36] M.C. García-Payo, M.A. Izquierdo-Gil, C. Fernández-Pineda, Wetting study of hydrophobic membranes via liquid entry pressure measurements with aqueous alcohol solutions, J. Colloid Interface Sci. 230 (2002) 420-431.

[37] K. Smolders, A.C.M. Franken, Terminology for Membrane Distillation, Desalination 72 (1989) 249-262.

[38] J. Zhang, J.D. Li, M. Duke, Z. Xie, S. Gray, Performance of asymmetric hollow fibre membranes in membrane distillation under various configurations and vacuum enhancement, J. Membr. Sci. 362 (2010) 517-528.

[39] M. Essalhi, M. Khayet, Self-sustained webs of polyvinylidene fluoride electrospun nano-fibers: Effects of polymer concentration and desalination by direct contact membrane distillation, J. Membr. Sci. 454 (2014) 133-143.

[40] M. Khayet, T. Matsuura, Determination of surface and bulk pore sizes of flat-sheet and hollow fiber membranes by atomic force microscopy, gas permetaion and solute transport methods, Desalination 158 (2003) 57-64.

[41] M. Khayet, M.C. García-Payo, F.A. Qusay, K.C. Khulbe, C.Y. Feng, T. Matsuura, Effects of gas gap type on structural morphology and performance of hollow fibers, J. Membr. Sci. 311 (2008) 259-269.

[42] M. Khayet, Membrane surface modification and characterization by X-ray photoelectron spectroscopy, atomic force microscopy and contact angle measurements, Appl. Surf. Sci. 238 (2004) 269-272.

[43] X. Tian, X. Jiang, Poly(vinylidene fluoride-co-hexafluoropropene) (PVDF-HFP) membranes for ethyl acetate removal from water, J. Hazard. Mater. 153 (2008) 128-135.

[44] M. Tazaki, R. Wada, M. Okabe, T. Homma, Crystallization and gelation of poly (vinylidene fluoride) in organic solvents, J. Appl. Polym. Sci. 65 (1997) 1517-1524.

[45] Z.K. Xu, L.Q. Shen, Q. Yang, F. Liu, S.Y. Wang, Y.Y. Xu, Ultrafiltration hollow fiber membranes from poly(ether imide): preparation, morphologies and properties, J. Membr. Sci. 223 (2003) 105-118.

[46] Q. Li, Z.L. Xu, M. Liu, Preparation and characterization of PVDF microporous membrane with highly hydrophobic surface, Polym. Adv. Technol. 22 (2011) 520-531.

[47] P. Zhang, Y. Wang, Z. Xu, H. Yang, Preparation of poly (vinyl butyral) hollow fiber ultrafiltration membrane via wet-spinning method using PVP as additive, Desalination 278 (2011) 186-193.

[48] D.T. Clausi, W.J. Koros, Formation of defect-free polyimide hollow fiber membranes for gas separations, J. Membr. Sci. 167 (2000) 79-89.

[49] H.A. Tsai, D.H. Huang, S.C. Fan, Y.C. Wang, C.L. Li, K.R. Lee, J.Y. Lai, Investigation of surfactant addition effect on the vapor permeation of aqueous ethanol mixtures through polysulfone hollow fiber membranes, J. Membr. Sci. 198 (2002) 245-258.

[50] C. Ma, C. Zhang, Y. Labreche, S. Fu, L. Liu, W.J. Koros, Thin-skinned intrinsically defect-free asymmetric mono-esterified hollow fiber precursors for crosslinkable polyimide gas separation membranes, J. Membr. Sci. 493 (2015) 252-262.

[51] Z. Wang, L. Sun, Q. Wang, B. Li, S. Wang, A novel approach to fabricate interconnected sponge-like and highly permeable polyvinylidene fluoride hollow fiber membranes for direct contact membrane distillation, Eur. Polym. J. 60 (2014) 262-272.

[52] S.H. Choi, F. Tasselli, J.C. Jansen, G. Barbieri, E. Drioli, Effect of the preparation conditions on the formation of asymmetric poly(vinylidene fluoride) hollow fibre membranes with a dense skin, Eur. Polym. J. 46 (2010) 1713-1725.

[53] J. Zhang, N. Dow, M. Duke, E. Ostarcevic, J.D. Li, S. Gray, Identification of material and physical features of membrane distillation membranes for high performance desalination, J. Membr. Sci. 349 (2010) 295-303.

[54] X. Zhang, J. Hu, Q. Chang, Y. Wang, J.e. Zhou, T. Zhao, Y. Jiang, X. Liu, Influences of internal coagulant composition on microstructure and properties of porous YSZ hollow fibre membranes for water treatment, Sep. Purif. Technol. 147 (2015) 337-345.

[55] M.C. García-Payo, M. Essalhi, M. Khayet, L. García-Fernández, K. Charfi, H. Arafat, Water desalination by membrane distillation using PVDF-HFP hollow fiber membranes, Membrane Water Treatment 1 (2010) 215-230.

[56] G. Wypych, Handbok of Polymers, ChemTec PUBLISHING, Toronto (2012).

[57] A. Moriya, T. Maruyama, Y. Ohmukai, T. Sotani, H. Matsuyama, Preparation of poly(lactic acid) hollow fiber membranes via phase separation methods, J. Membr. Sci. 342 (2009) 307-312.

[58] L. García-Fernández, M.C. García-Payo, M. Khayet, Mechanism of formation of hollow fiber membranes for membrane distillation: 2. Outer coagulation power effect on morphological characteristics, J. Membr. Sci. Submitted.

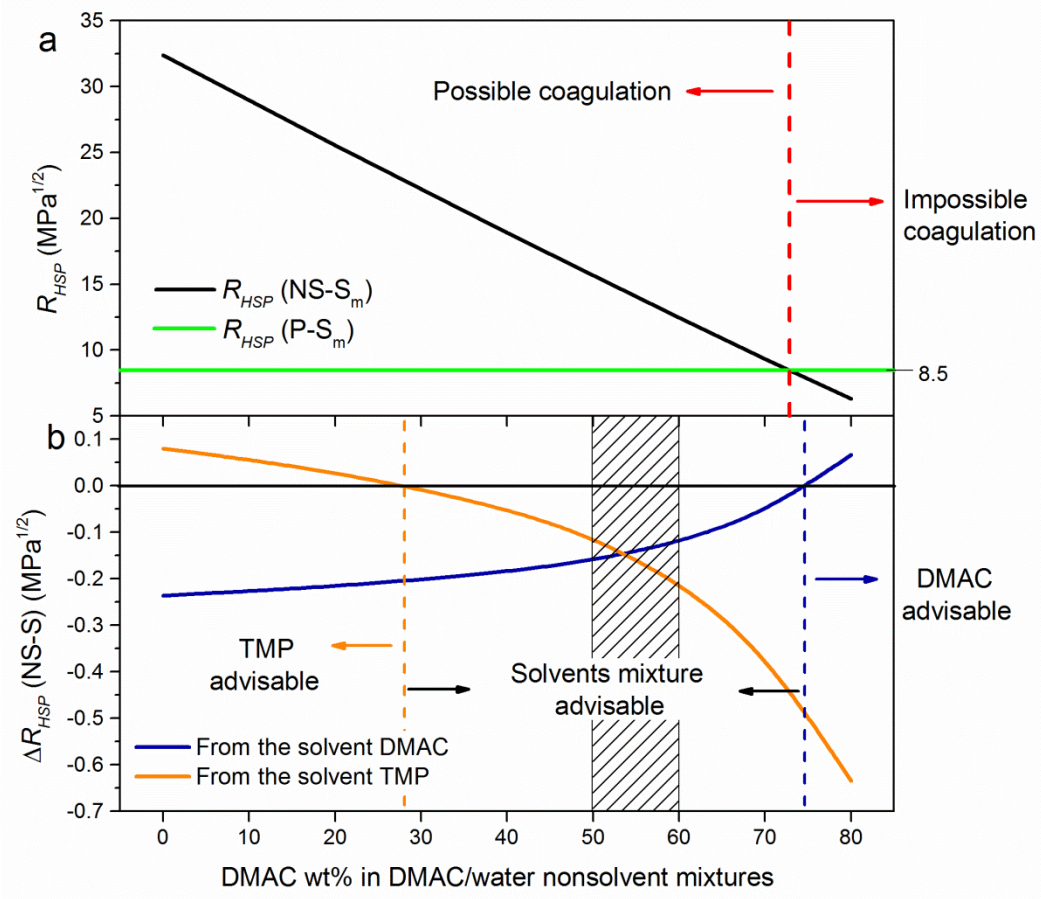

Fig. 1. Effect of the DMAC content in DMAC/water nonsolvent mixtures (a) on the R_{HSP} (NS-S_m) and (b) on the ΔR_{HSP} (NS-S).

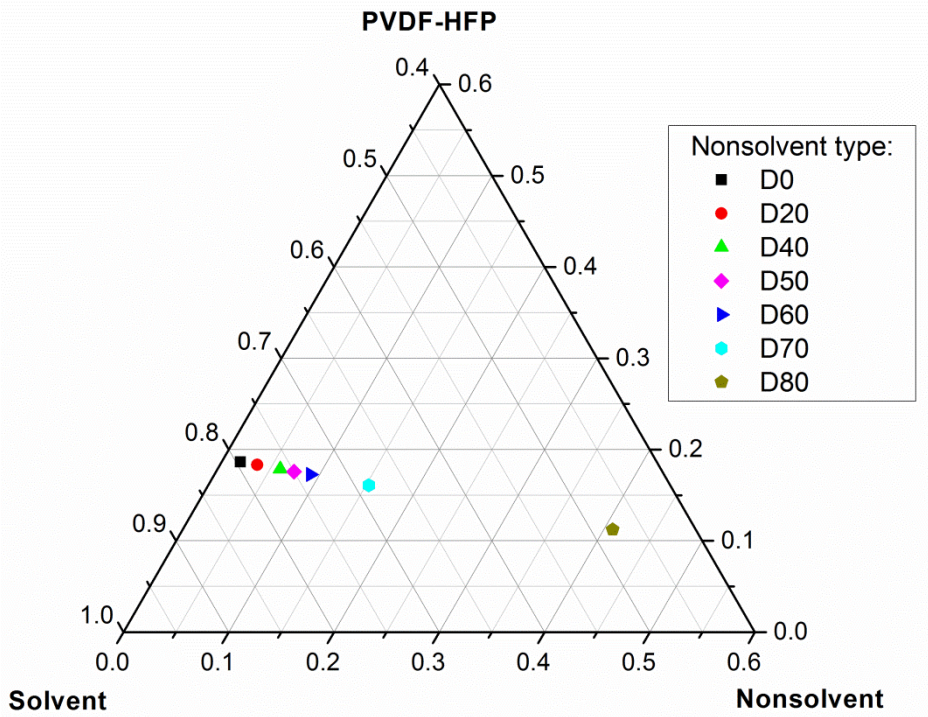

Fig. 2. Ternary phase diagram of the copolymer/solvent/nonsolvent systems.

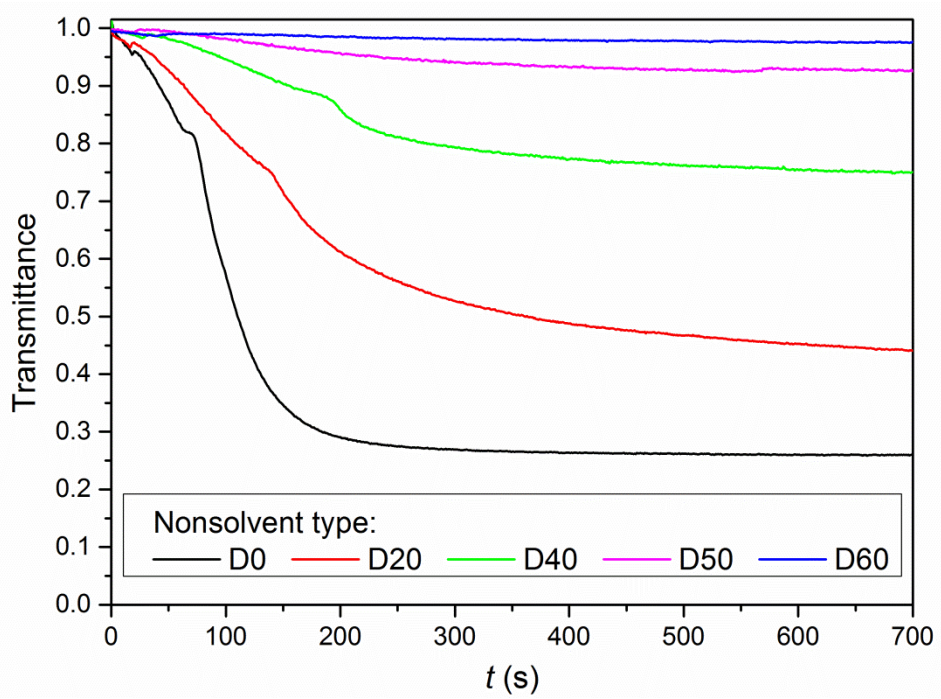

Fig. 3. Coagulation experiments of the spinning solution for different nonsolvent mixtures (DMAC/water in different proportions).

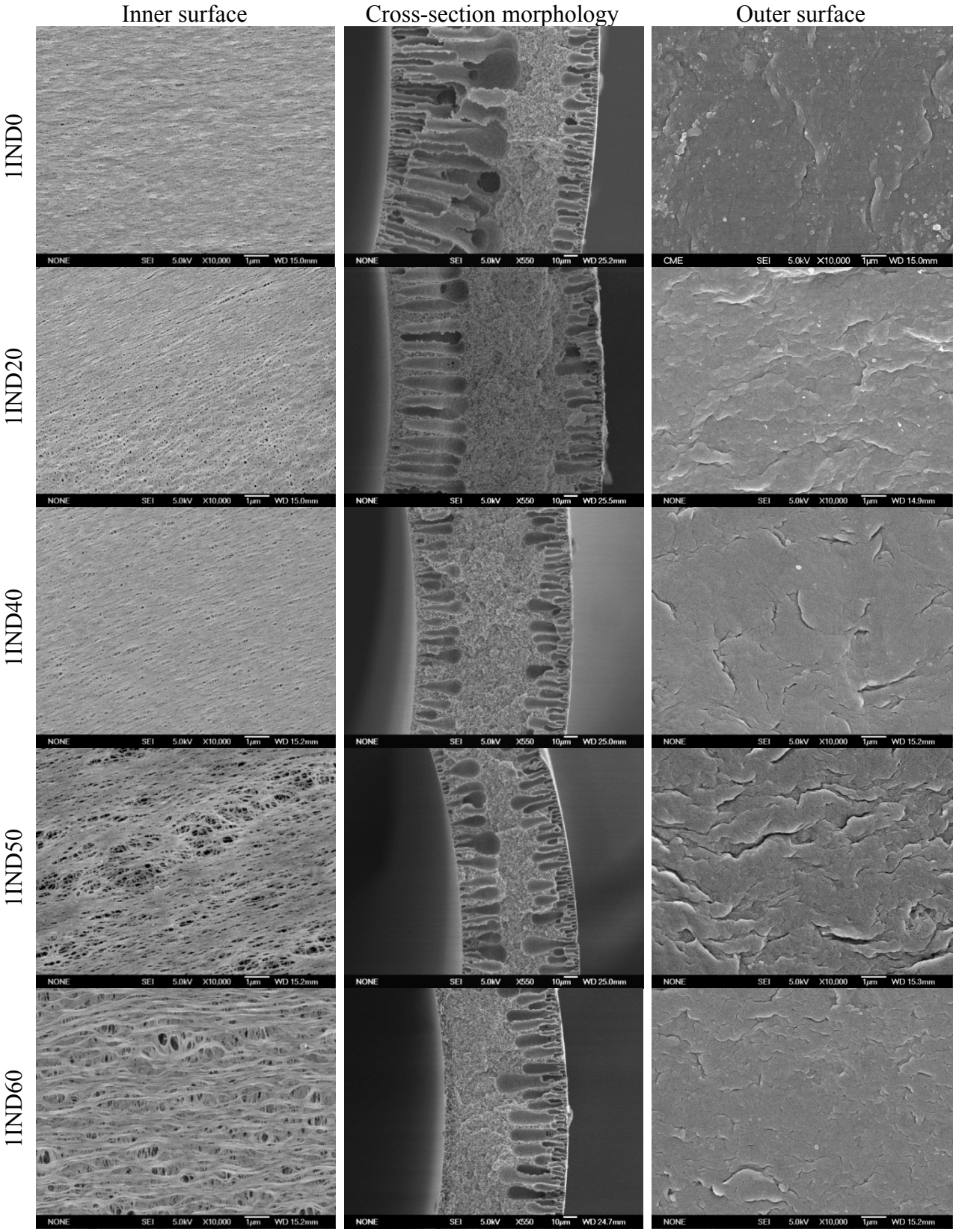

Fig. 4. SEM images of the cross-section morphology and the inner and outer surfaces of the hollow fiber membranes prepared with different concentrations of DMAC in water as internal coagulants.

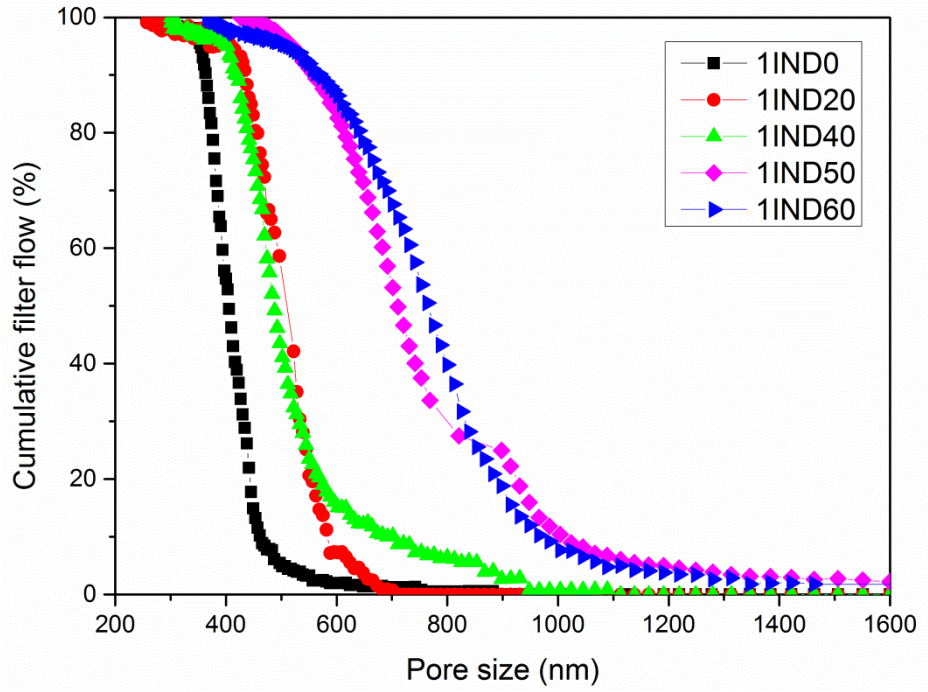

Fig. 5. Cumulative filter flow of the hollow fiber membranes prepared with different DMAC concentrations in water as internal coagulants.

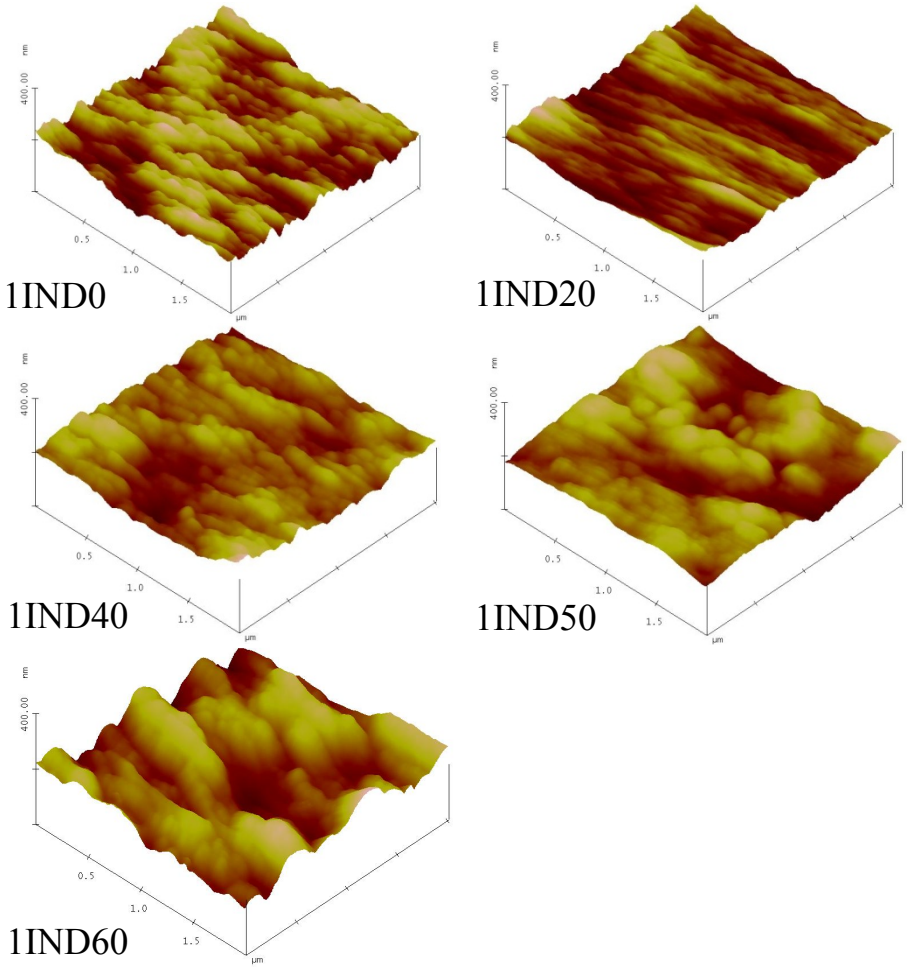

Fig. 6. 3D AFM images of the inner surfaces of the hollow fiber membranes prepared with different concentrations of DMAC in water as internal coagulants.

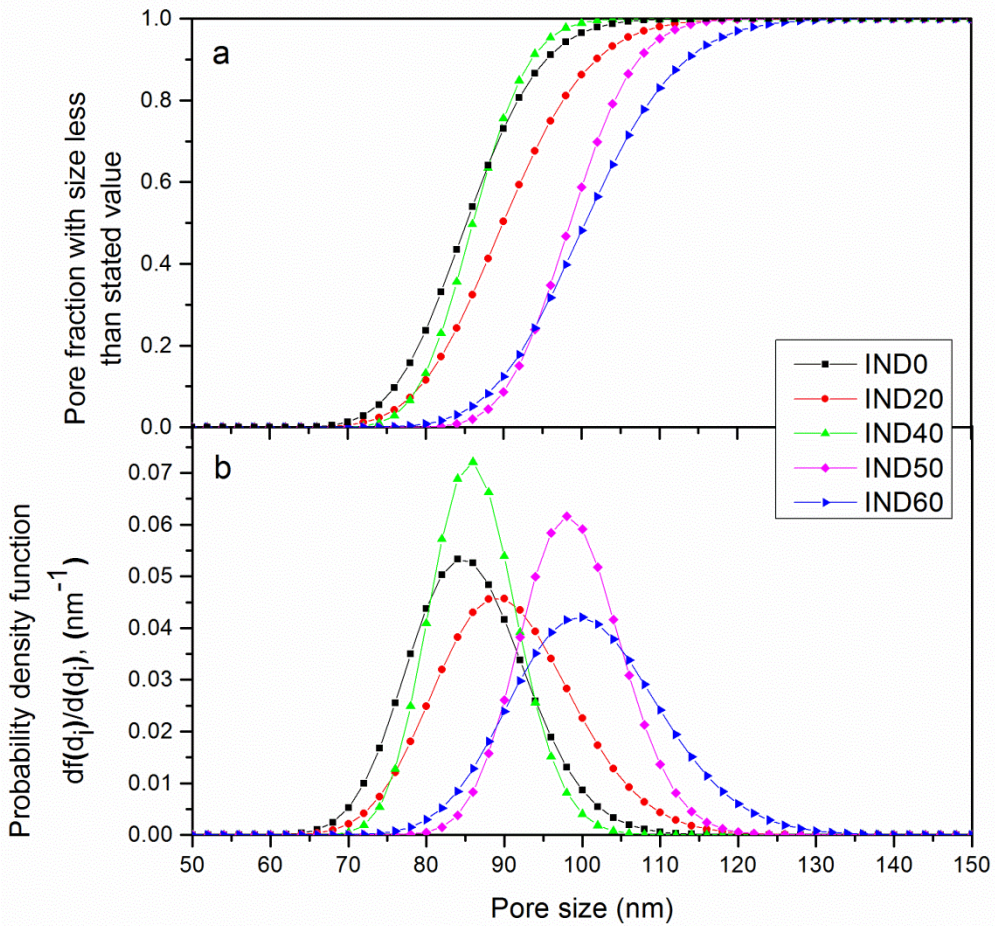

Fig. 7. Cumulative pore size (a) and probability density function (b) curves generated from the pore sizes obtained from AFM images of the inner surfaces of the hollow fiber membranes prepared with different DMAC concentrations in water as internal coagulants.

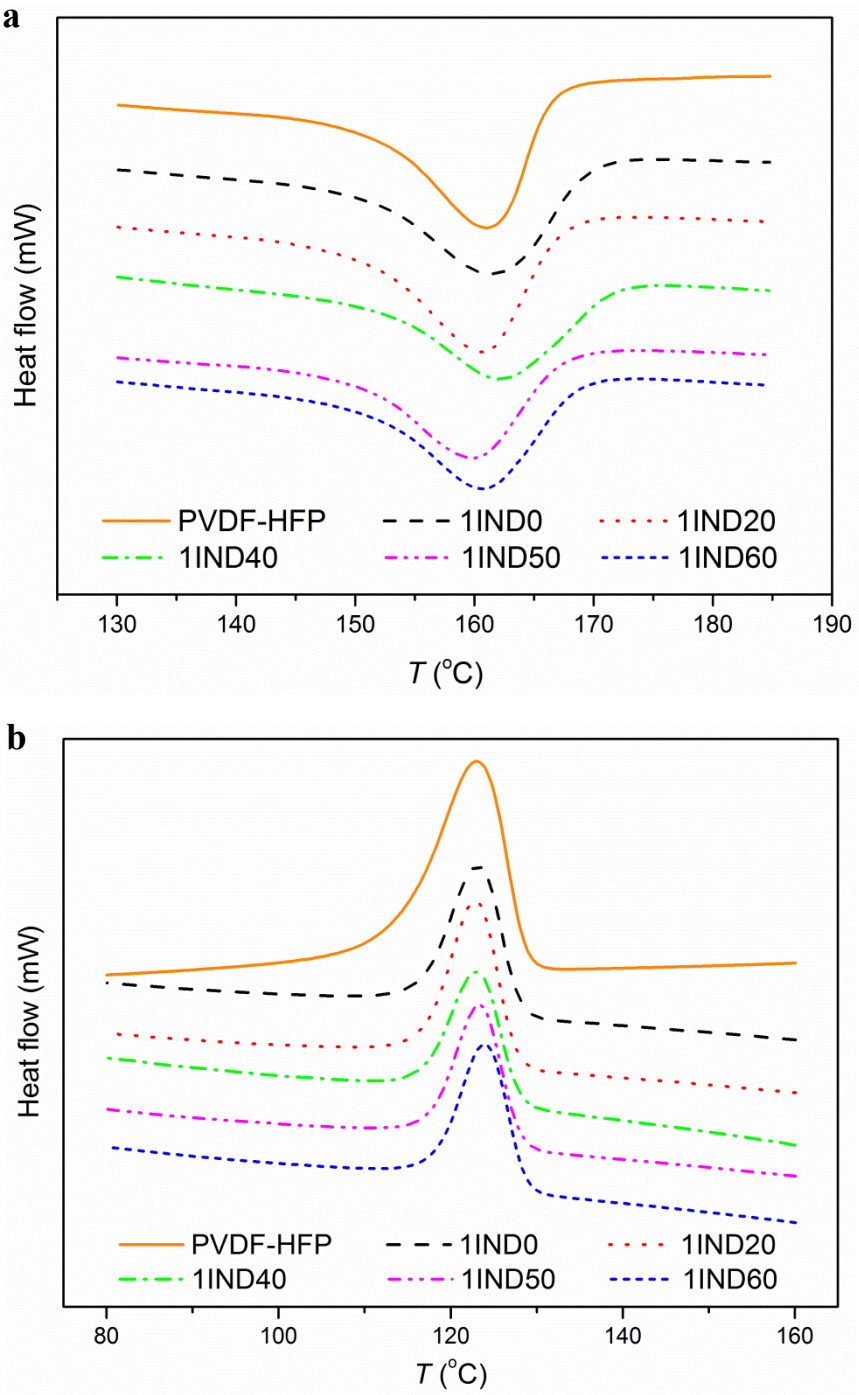

Fig. 8. DSC thermograms, (a) heating and (b) cooling of the copolymer PVDF-HFP and the hollow fiber membranes prepared with different concentrations of DMAC in water as internal coagulants.

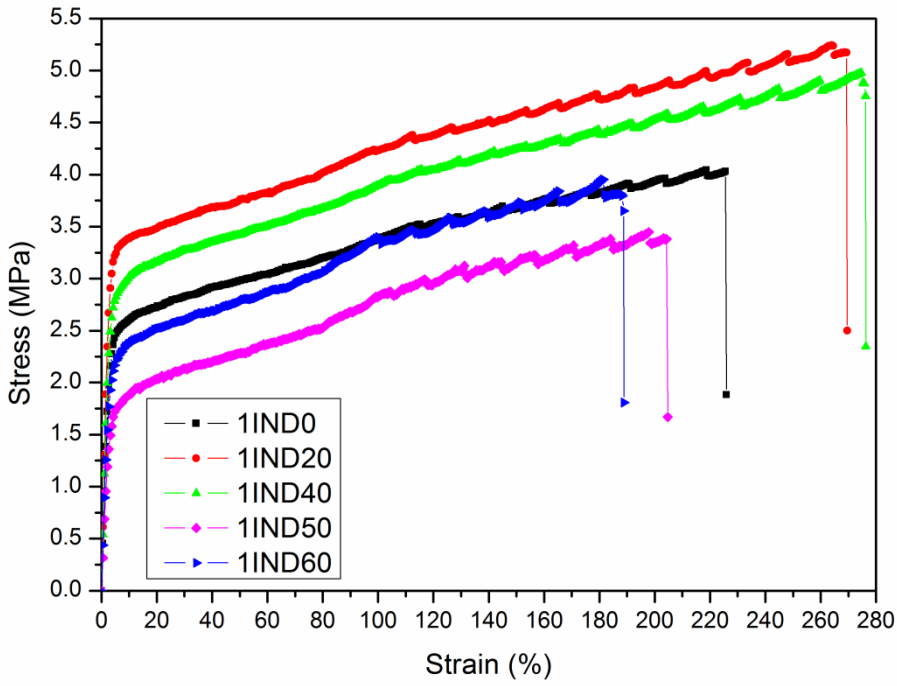

Fig. 9. Stress-strain curves of the hollow fiber membranes prepared with different DMAC amounts in water as internal coagulants.

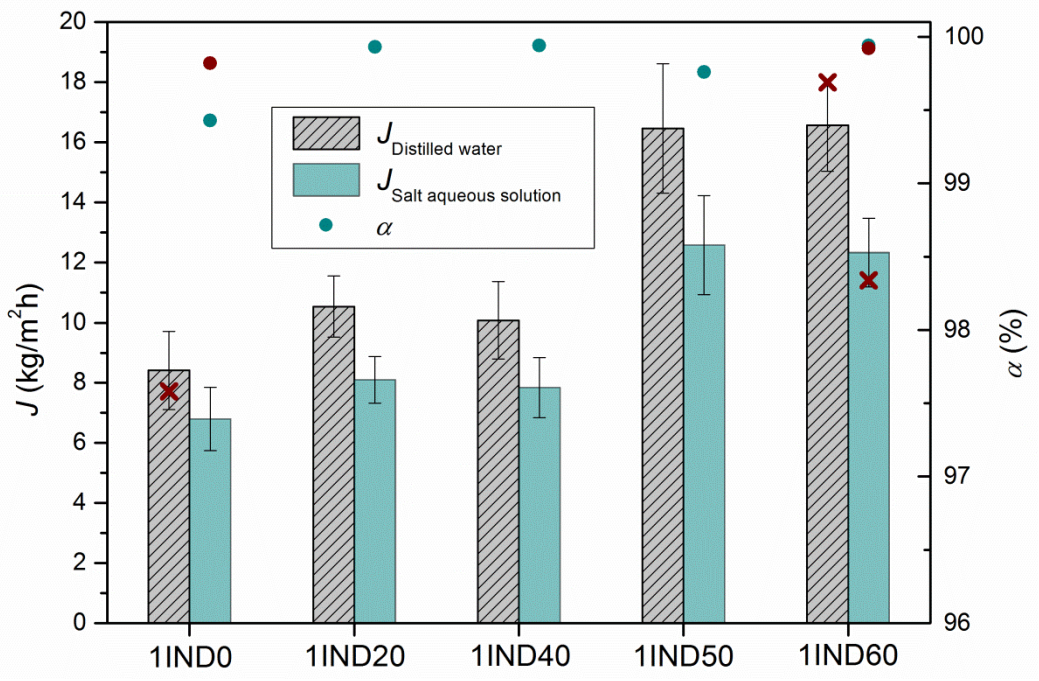

Fig. 10. DMCD permeate flux and salt rejection factor of the hollow fiber membranes prepared with different DMAC amounts in water as internal coagulants. (Feed temperature = 80 °C; Permeate temperature = 25 °C). **X** represents the DCMD permeate flux and ● the salt rejection factor of hollow fiber membranes prepared in different batches.

Table 1. Spinning parameters of PVDF-HFP hollow fiber membranes.

Parameters	Operating conditions
Spinneret: 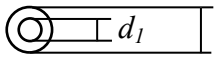	d_1= 1.0 mm / d_2= 2.4 mm
Extrusion pressure (kPa)	60
Polymeric solution temperature (ºC)	42
Internal coagulant	DMAC/distilled water
Internal coagulation temperature (ºC)	42
Internal coagulant flow rate (m^3/s)	$2.7\ 10^{-7}$
Air gap distance (m)	0.275
Liquid coagulation bath	Tap water
Liquid coagulation bath temperature (ºC)	42

Table 2. Solubility parameters of the solvents, the solvents mixture, the additive PEG, the nonsolvent (water and DMAC/water mixtures) and PVDF-HFP with their *HSP* distances (R_{HSP}).

Material type	Code	Composition: material (wt%)			Solubility parameters ($MPa^{1/2}$)			R_{HSP} ($MPa^{1/2}$) [16, 27]	
		Compound 1	Compound 2	Compound 3	δ_D	δ_P	δ_H	P-S [ii]	NS- S_m [iii]
Copolymer (P)	PVDF-HFP [28]	---	---	---	15.3	7.2	5.3	---	---
Additive	PEG [10]	---	---	---	15.3	9.6	8.5	---	---
Solvents	DMAC [27]	---	---	---	16.8	11.5	10.2	7.2	---
	TMP [27]	---	---	---	16.7	15.9	10.2	10.4	---
Solvent mixture (S_m)	DMAC40 [i]	DMAC (40%)	TMP (60%)	PEG (5%)	16.7	13.6	10.1	8.5	---
Nonsolvent (NS)	Water (D0)	DMAC (0%)	Water (100%)	---	15.5	16	42.3	---	32.4
	D20	DMAC (20%)	Water (80%)	---	15.8	15	35.5	---	25.5
	D40	DMAC (40%)	Water (60%)	---	16	14.1	28.9	---	18.9
	D50	DMAC (50%)	Water (50%)	---	16.2	13.7	25.7	---	15.6
	D60	DMAC (60%)	Water (40%)	---	16.3	13.2	22.5	---	12.5
	D70	DMAC (70%)	Water (30%)	---	16.4	12.8	19.4	---	9.3
	D80	DMAC (80%)	Water (20%)	---	16.5	12.3	16.3	---	6.3

[i] Calculated using Eq. (1).
[ii] P-S: PVDF-HFP-solvent interaction.
[iii] NS-S_m: nonsolvent-mixed solvent interaction.

Table 3. Diameters, thickness, void volume fraction, *LEP* and contact angles of hollow fiber membranes prepared with different amounts of DMAC in water as internal coagulants.

Membrane	Inner diameter (μm)	Outer diameter (μm)	Thickness (μm)	Void volume fraction (ε %)	*LEP* (10^5 Pa)	Inner contact angle (^{o})	Outer contact angle (^{o})
1IND0	1190 ± 180	1550 ± 150	180 ± 40	66.0 ± 2.4	1.02 ± 0.06	152.2 ± 1.3	95.8 ± 0.4
1IND20	994 ± 96	1332 ± 94	169 ± 28	53.0 ± 0.7	3.93 ± 0.20	147.5 ± 1.8	99.1 ± 0.4
1IND40	1360 ± 170	1630 ± 160	133 ± 30	62.5 ± 0.5	2.85 ± 0.21	142.6 ± 0.7	89.2 ± 0.7
1IND50	1120 ± 150	1310 ± 150	99 ± 24	76.3 ± 2.2	1.69 ± 0.19	157.7 ± 1.6	90.0 ± 0.6
1IND60	1180 ± 110	1380 ± 110	96 ± 17	78.4 ± 0.8	1.35 ± 0.34	149.8 ± 0.6	89.4 ± 0.6

Table 4. Bubble pore size, mean pore size, and smallest pore size of the hollow fiber membranes prepared with different amounts of DMAC in water as internal coagulants determined by gas-liquid porosimetry.

Membrane	Bubble pore size (nm)	Mean pore size (nm)	Smallest pore size (nm)
1IND0	566 ± 6	403 ± 3	356 ± 2
1IND20	586 ± 6	488 ± 4	400 ± 3
1IND40	819 ± 13	474 ± 4	403 ± 3
1IND50	1273 ± 30	656 ± 8	492 ± 4
1IND60	1989 ± 74	711 ± 9	528 ± 5

Table 5. Minimum, maximum and average mean roughness parameter, R_a, together with the corresponding standard deviation of the internal and external surfaces of the hollow fibers prepared with different concentrations of DMAC in water as internal coagulants (scan range considered 2μm × 2μm).

Membrane	R_a (nm) Inner surface			R_a (nm) Outer surface		
	Minimum	Maximum	Average	Minimum	Maximum	Average
1IND0	13.4	17.4	16.0 ± 1.2	16.7	26.3	21.0 ± 4.0
1IND20	7.3	11.5	9.1 ± 1.3	16.0	24.1	19.4 ± 3.0
1IND40	9.5	14.6	12.0 ± 2.0	15.3	22.6	18.4 ± 2.5
1IND50	10.2	20.8	13.7 ± 2.8	17.9	25.2	21.4 ± 2.6
1IND60	20.0	26.1	22.8 ± 2.1	11.8	25.3	16.0 ± 4.0

Table 6. Mean pore size, μ_p, and geometric standard deviation, σ_p, of the internal surfaces of the hollow fiber membranes prepared with different concentrations of DMAC in water as internal coagulants.

Membrane	μ_p(nm)	σ_p(nm)
1IND0	85.23	1.09
1IND20	89.91	1.10
1IND40	86.04	1.07
1IND50	98.53	1.07
1IND60	100.44	1.10

Table 7. Melting temperature (T_m), crystallization temperature (T_c), enthalpy of melting (ΔH_m), enthalpy of crystallization (ΔH_m) and crystallinity (X_c) of the copolymer PVDF-HFP and the hollow fiber membranes prepared with different DMAC concentrations in water as internal coagulants.

Sample	Heating process		Cooling process		Crystallinity
	$\Delta H_m \pm 0.5$ (J/g)	$T_m \pm 0.15$ (°C)	$\Delta H_c \pm 0.5$ (J/g)	$T_c \pm 0.15$ (°C)	X_c (%)
PVDF-HFP	45.7	160.98	45.4	123.00	43.6
1IND0	45.5	161.49	45.5	123.48	43.4
1IND20	45.6	160.71	45.4	123.00	43.6
1IND40	45.2	162.18	45.3	123.21	43.2
1IND50	45.3	159.97	45.5	123.48	43.3
1IND60	45.4	160.69	45.6	124.25	43.4

Table 8. Mechanical properties (Young´s modulus, E; yield stress, σ_y; tensile stress at break, σ_b and strain at break, ε_b) of the hollow fiber membranes prepared with different DMAC concentrations in water as internal coagulants.

Membrane	E (MPa)	σ_y (MPa)	σ_b (MPa)	ε_b (%)
1IND0	103 ± 9	1.83 ± 0.09	4.26 ± 0.20	230 ± 23
1IND20	135 ± 9	2.41 ± 0.02	5.4 ± 0.5	267.3 ± 2.8
1IND40	117 ± 7	2.27 ± 0.23	5.0 ± 0.4	269 ± 10
1IND50	62 ± 6	1.15 ± 0.08	3.30 ± 0.07	212 ± 11
1IND60	87 ± 3	1.55 ± 0.14	3.70 ± 0.21	195 ± 9

Highlights:

Nonsolvent coagulation power efficiency can be determined via Hansen solubility analysis.

Concentration of solvent in the nonsolvent mixture affects the thermodynamic and kinetics experiments.

Open-porous inner surfaces with larger pores were obtained with greater amount of DMAC in the internal coagulant.

DCMD flux was almost doubled using 50 and 60 wt% of DMAC in water as a bore liquid.